PHOTOTHERMAL IMAGING OF INDENTATION IN SILICON NITRIDE

Final Technical Report

Kyrill L. Muratikov, Alexej L. Glazov

September 1996

United States Army

EUROPEAN RESEARCH OFFICE OF THE U.S. ARMY

London England

CONTRACT NUMBER 68171 - 95 - C - 9134

Ioffe Physico - Technical Institute

Russian Academy of Sciences

Approved for Public Release; distribution unlimited

Table of Contents

COVER SHEET OF REPORT

ABSTRACT 1

REPORT NARRATIVE.....2

Statement of the Problem.....2

Background and Significance 2

Approaches to the Problem 3

Theoretical Part 3

Experimental Set - Up and Results 8

Conclusions and Recommendations 9

Literature Cited 9

ABSTRACT

Theoretical model for determination of temperature distribution in ceramics with a lateral crack is developed for a case of photothermal measurements of indentation cracks. The lateral crack is modeled by a horizontal buried layer with a given thermal resistance. A possible penetration of the pump beam light in ceramics is taken into account. The dependence of photoacoustic and photodeflection signals on the thermal resistance and pump beam light in ceramics are investigated. Photodeflection and piezoelectric images of indentation cracks in silicon nitride have been obtained. It is shown that these images have different structure and can be used for the development of a complex approach to the problem of indentation crack imaging in silicon nitride ceramics.

List of keywords: photothermal imaging, indentation, ceramics, crack

REPORT NARRATIVE

Statement of the problem

The problem of crack diagnostics and imaging in advanced ceramics (silicon nitride) is of great importance for understanding the fracture processes in these materials [1,2]. An indentation contact provides a reproducible procedure for crack generation in brittle materials. The most detailed information about crack structure is obtained at present only for optically transparent materials in a highly polished form with the help of optical methods [2]. Unfortunately, few of advanced ceramics (including silicon nitride) are fully transparent. Therefore optical methods are not able to provide full information about cracks in these materials.

For diagnostics of advanced ceramics other nondestructive methods or a combination of them should be used. Photoacoustic gas microphone and photodeflection methods appeared to be powerful techniques for defect diagnostics and imaging in ceramics [3-6]. Some preliminary results about possibility of monitoring the residual stress field distribution around an indentation in ceramic samples based on silicon nitride has been obtained by photoacoustic method with a piezoelectric transducer [7]. Unfortunately, the application of photothermal methods to advanced ceramics nondestructive evaluation has more qualitative character than quantitative one up to now. Therefore, in this report besides of an experimental imaging of indentation cracks in advanced ceramics by photothermal methods a great attention is paid to the development of a model for quantitative photothermal measurements of lateral cracks.

Background and significance

Advanced ceramics have been extensively studied during the last years, because of the unique combination of such parameters as hardness, wear tolerance, corrosion resistance, high temperature capability and low density. The investigation of these materials has both a scientific and applied value. From the scientific point of view, the consideration of the indentation-induced crack system and arising stress fields are of great value for understanding elastic-plastic and fracture properties [1,2]. From the applied point of view, these investigations are of importance for the determination of the quality of ceramics, optimization of machining and working conditions, diagnostics of wear [8]. At present advanced ceramics are being applied in new Detroit Diesel engines and in accordance with the Advance Ceramic Technology Insertion Program for the Self Propelled Howitzer. It is hoped that the exploration of the lateral crack system of ceramic alloys will lead to a figure of merit for materials to be used for bearings [5].

Nondestructive techniques for reliably detecting and accurately sizing cracks are an essential requirement for damage tolerant design. There are limitations on using optical, X-ray, ultrasonic techniques and techniques based on electric conductivity and magnetic properties for nondestructive testing of ceramics. Purely optical methods are usually not effective for subsurface defect detection because of the strong absorption and scattering of light in ceramics. The contrast of X-ray images of small holes and cracks with a length of the order 0.1 mm in the light elements comprising most ceramics such as silicon nitride is very poor. The main difficulties in the application of ultrasonic techniques are connected with understanding the reflection for complex crack systems. Methods based on electric conductivity or magnetic properties like eddy current tests can only rarely be used because the magnetic susceptibility and electric conductivity of most ceramics is very poor. These problems stimulate the development of photothermal microscopy methods for diagnostics of ceramics.

Approaches to the problem

In this report both theoretical and experimental investigations of indentation cracks in silicon nitride are performed.

The main purpose of the theoretical part is to develop a basis for quantitative photothermal measurements of lateral cracks in silicon nitride. In the theoretical part of the report analytical model for the lateral crack in ceramics is provided. In this model the lateral crack is considered as a thermal resistance between two parallel layers of the material. The formulation of this model in terms of reflection and transmission coefficients proposed by F.Lepoutre, et. al. [9] is also provided. In the model the possible effect of pump beam light penetration in ceramics is taken into account. On the base of this model the behavior of photoacoustic gas microphone and photodeflection signals for the case of lateral crack imaging in ceramics is analyzed.

In the experimental part of the report two-dimensional point by point measurement of indentation crack system is performed by photothermal methods. A specific feature of the approach used in this proposal that both normal and transverse components of photodeflection signal are measured. Photoacoustic imaging with piezoelectric signal detection of indentation crack system is also within the framework of this report.This approach provides a new possibility to detect lateral and vertical cracks, residual stress field distribution around indentation in one measuring procedure. It gives also an additional information about parameters of the crack system because of these signals are the independent quantities. By performing this procedure under different modulation frequencies it is possible to obtain depth information of the crack structure and residual stresses.

Theoretical part

For determination of the properties of photoacoustic and photodeflection signals let us consider the model of the lateral crack as a horizontal buried layer with a given thermal resistance. The configuration of the sample with the lateral crack, positions of the probe and pump laser beams for the case of photodeflection measurement are shown in Fig.1. In this model we take into account possible penetration of the pump beam light into the first layer. However, it is assumed that this light does not penetrate into the second layer.

For this case thermal equations for the layers one and two can be written in the following form

$$\frac{\partial T_g}{\partial t} = \kappa_g \Delta T_g \ , \tag{1}$$

$$\frac{\partial T_1}{\partial t} = \kappa_1 \Delta T_1 + \frac{\kappa_1 \alpha I_p(x,y,t) e^{-\alpha z}}{K_1} \ , \tag{2}$$

$$\frac{\partial T_2}{\partial t} = \kappa_2 \Delta T_2 \ , \tag{3}$$

where κ_g , κ_1 and κ_2 are the thermal diffusivities of the air, layers 1 and 2; K_1 is the thermal conductivity of the first layer, α is the coefficient of the pump light absorption in the first layer; $I_p(x,y,t)$ is the distribution of the pump beam intensity on the surface of the sample, absorbed by the sample.

Our assumption about a depth of the pump light penetration in the sample means that the equation is valid at $\alpha d \geq 1$. Boundary conditions taking into account the thermal resistance between layers can be expressed by the following expressions

$$T_1 = T_2|_{z=0}\ , \quad K_1\frac{\partial T_1}{\partial z} = K_g\frac{\partial T_g}{\partial z}\ |_{z=0}\ ,$$

$$K_1\frac{\partial T_1}{\partial z} = K_2\frac{\partial T_2}{\partial z}\ |_{z=d}\ , \quad T_1 - T_2 = -R_t K_1\frac{\partial T_1}{\partial z}\ |_{z=d}\ , \tag{4}$$

where K_1 and K_2 are the thermal conductivities of the air and layer 2; is the thermal resistance between layers.

For solution of eqs.(1), (2) and (3) let us use the Fourier transform and represent all temperatures in the form

$$T(x,y,z,t) = \int dk_x \int dk_y e^{ik_x x + ik_y y}\hat{T}(k_x,k_y,z,t)\ , \tag{5}$$

where $\hat{T}(k_x,k_y,z,t)$ is the Fourier transform of the temperature over coordinates x and y.

In this report a generation of thermal waves by periodic heart source is assumed. Therefore, the dependence of the temperatures on the time can be used in the form $e^{i\omega t}$. In this case, the equation for the Fourier transform, for example in the first layer, is given by

$$i\omega\hat{T}_1(k_x,k_y,\omega) = \kappa_1\left(-k_x^2 - k_y^2 + \frac{\partial^2}{\partial z^2}\right)\hat{T}_1(k_x,k_y,\omega) + \frac{\kappa_1\alpha\hat{I}_p(k_x,k_y)e^{-\alpha z}}{K_1}, \tag{6}$$

where $\hat{I}_p(k_x,k_y)$ is the Fourier transform of the pump beam light distribution on the surface of the sample. Equations for $\hat{T}_g$ and $\hat{T}_2$ have the similar form.

For a Gaussian profile of the pump beam intensity distribution

$$I_p(x,y) = \frac{W_0}{\pi a^2}e^{-\frac{x^2+y^2}{a^2}}$$

the result for $\hat{I}_p(k_x,k_y)$ is given by

$$\hat{I}_p(k_x,k_y) = \frac{W_0}{(2\pi)^2}e^{-\frac{a^2(k_x^2+k_y^2)}{4}}\ ,$$

where a is the radius and W_0 is the power of the pump laser beam.

For determination of the photoacoustic signal in experiments with a gas microphone cell or the photodeflection signal it is necessary to know a temperature distribution in a gas near the sample. When this temperature is known the photoacoustic signal is given by

$$P(\omega) = C_p\int dx\int dy T_g(x,y,z,\omega)\big|_{z=0}\ , \tag{7}$$

where C_p is the proportionality coefficient.

By using eq.(5) this equation can be transformed to the form

$$P(\omega) = C_p(2\pi)^2\hat{T}_g(0,0,z,\omega)\big|_{z=0}\ . \tag{8}$$

The normal and transverse components of the photodeflection signal are connected with the Fourier transform of the temperature $T_g(x,y,z,\omega)$ by equations [10,11]

$$S_n = \frac{C_s I_0}{\lambda r\sqrt{\pi}}\frac{\partial n}{\partial T}\int_0^{\infty} dz \int_{-\infty}^{\infty} dk_y \hat{T}_g(0,k_y,0,\omega) erfi(\frac{z-z_0}{r\sqrt{2}})\times$$
$$\exp\left[ik_y y_0 - \gamma_g z - \frac{k_y^2 r^2}{4} - \frac{(z-z_0)^2}{r^2}\right], \tag{9.1}$$

$$S_t = \frac{C_s I_0}{2\lambda r\sqrt{\pi}}\frac{\partial n}{\partial T}\int_0^{\infty} dz \int_{-\infty}^{\infty} dk_y \hat{T}_g(0,k_y,0,\omega) erfi(\frac{y-y_0}{r\sqrt{2}})\left[1+erf(\frac{z_0}{r}-\frac{\gamma_g r}{2})\right]\times$$
$$\exp\left[ik_y y_0 - \gamma_g z_0 + \frac{\gamma_g^2 r^2}{4} - \frac{(y-y_0)^2}{r^2}\right], \tag{9.2}$$

where C_s is the proportionality coefficient, I_0 is the intensity of the probe laser beam, λ is the wave length of the probe laser light, $\gamma_g = \sqrt{k_y^2 + \frac{i\omega}{\kappa_g}}$, r is the radius of the probe beam in the focus, $\frac{\partial n}{\partial T}$ is the derivative of the medium refractive index with respect to temperature in the vicinity of the object, y_0 is the transverse shift of the probe laser beam relative to the thermal lens, z_0 is the height at which the probe beam propagates over the surface of the object,

$$erfi(x) = \frac{2}{\sqrt{\pi}}\int_0^x \exp(x^2)dx\,,\quad erf(x) = \frac{2}{\sqrt{\pi}}\int_0^x \exp(-x^2)dx\,.$$

Therefore, in accordance with eqs.(8) and (9) the photoacoustic signal and photodeflection signals can be determined if the surface temperature of the sample is known.

The temperature distribution in the air, layers 1 and 2 can be determined from eqs.(1),(2) and (3) and boundary conditions (4)

$$\hat{T}_g(k_x,k_y,z,\omega) = Ge^{q_g z}\,, \tag{10.1}$$

$$\hat{T}_1(k_x,k_y,z,\omega) = F_1 e^{q_1 z} + F_2 e^{-q_1 z} + Ae^{-\alpha z}\,, \tag{10.2}$$

$$\hat{T}_2(k_x,k_y,z,\omega) = Se^{-q_2 z}\,, \tag{10.3}$$

where $q_g = \sqrt{\frac{i\omega}{\kappa_g} + k_x^2 + k_y^2}$, $q_{1,2} = \sqrt{\frac{i\omega}{\kappa_{1,2}} + k_x^2 + k_y^2}$,

$$G = A\left(\cosh q_1 d\frac{q_1 K_1 P e^{-\alpha d} - N(\alpha K_1 + q_g K_g)}{NM + q_1 K_1} + 1\right),$$

$$A = \frac{\kappa_1 \alpha \hat{I}_p}{K_1}\frac{1}{\frac{i\omega}{\kappa_1} + k_x^2 + k_y^2 - \alpha^2},$$

$$F_1 = \frac{1}{2}\frac{A}{NM + q_1 K_1}\left[\left(\alpha K_1 + q_g K_g\right)\left(1 - Ne^{-q_1 d}\right) + Pe^{-\alpha d}\left(M + q_1 K_1 e^{-q_1 d}\right)\right],$$

$$F_2 = \frac{1}{2}\frac{A}{NM + q_1 K_1}\left[-\left(\alpha K_1 + q_g K_g\right)\left(1 + Ne^{q_1 d}\right) + Pe^{-\alpha d}\left(q_1 K_1 e^{q_1 d} - M\right)\right],$$

$$S = -\frac{q_1 K_1}{q_2 K_2}\frac{MA}{NM + q_1 K_1} e^{q_2 d}\cosh q_1 d\left(\frac{\alpha K_1 + q_g K_g}{M} + Pe^{-\alpha d}\right) + \frac{\alpha K_1 A}{q_2 K_2} e^{-(\alpha + q_2)d},$$

$$M = q_g K_g \cosh q_1 d + q_1 K_1 \sinh q_1 d ,$$

$$N = \sinh q_1 d + (1 + R_t q_2 K_2)\frac{q_1 K_1}{q_2 K_2}\cosh q_1 d ,$$

$$P = \frac{\alpha K_1}{q_2 K_2}(1 + R_t q_2 K_2) - 1 .$$

Setting z=0 one can obtain the surface temperature of the sample from the temperature distribution in the air or in the layer 1. Therefore, the problem of the photoacoustic and photodeflection signals determination is solved by eqs.(8), (9) and (10). Unfortunately, it is impossible to get photodeflection signals in analytical form. Therefore, a program for computer calculation of the photodeflection signals has been developed.

The problem of heat transport in a sample with a lateral crack can be formulated in terms of reflection and transmission coefficients for thermal waves. We extended the approach developed by F.Lepoutre [9] and D.Rose [12] to this case taking into account thermal resistance between layers and possible penetration of the pump beam light inside the sample.

The transmission and reflection coefficients are defined as the ratio of the transmitted or reflected wave amplitude to the incident wave amplitude (at the boundary) [12]. The incident and reflected waves on side 1 of the boundary $z = d$ and the transmitted wave on side 2 of the boundary $z = d$ are described, respectively, by

$$\hat{I}_1(k_x, k_y, z) = C_I e^{q_1 z} \qquad \text{for } 0 \le z \le d , \tag{11.1}$$

$$\hat{R}_1(k_x, k_y, z) = C_R e^{-q_1 z} \qquad \text{for } 0 \le z \le d , \tag{11.2}$$

$$\hat{T}_2(k_x, k_y, z) = C_T e^{q_2 z} \qquad \text{for } d \le z \le \infty. \tag{11.3}$$

Eq.(11.1) corresponds to the incident plane wave with the wave vector (k_x,k_y); eq.(11.2) corresponds to the reflected plane wave for the incident wave with the wave vector (k_x,k_y); eq.(11.3) corresponds to the transmitted plane wave with the wave vector (k_x,k_y). In eqs.(11.1) and (11.2) the term $Ae^{-\alpha z}$ from eq.(10.2) is not taken into account. This term corresponds to a direct heating of the sample by the absorbed pump light energy and does not represent any thermal wave.

The temperature in layer 1 is

$$\hat{T}_1(k_x, k_y, z) = C_I e^{q_1 z} + C_R e^{-q_1 z} \tag{12.1}$$

and the temperature in layer 2 is

$$\hat{T}_2(k_x, k_y, z) = C_T e^{q_2 z} . \tag{12.2}$$

In accordance with the definition [12] reflection and transmission coefficients are equal to

$$\hat{R}_{12}(k_x, k_y) = \frac{\hat{R}_1(k_x, k_y, d)}{\hat{I}_1(k_x, k_y, d)} = \frac{C_R}{C_I} , \tag{13.1}$$

$$\hat{T}_{12}(k_x, k_y) = \frac{\hat{T}_2(k_x, k_y, d)}{\hat{I}_1(k_x, k_y, d)} = \frac{C_T}{C_I} . \tag{13.2}$$

Setting $k_x = k_y = 0$ in eqs.(11) and (13) one obtains the incident, reflected and transmitted waves and reflection and transmission coefficients for one dimensional case.

Using boundary conditions (4) and eqs.(12.1), (12.2) one can calculate the reflection and transmission coefficients

$$\hat{R}_{12} = \frac{1-\xi_{12}(1-R_t q_1 K_1)}{1+\xi_{12}(1+R_t q_1 K_1)}, \qquad \hat{T}_{12} = \frac{2}{1+\xi_{12}+R_t q_2 K_2}, \tag{14}$$

where $\xi_{12} = \frac{q_2 K_2}{q_1 K_1}$ is the ratio of effusivities of layer 1 and layer 2.

For the case $R_t = 0$ these expressions agree with the results for the reflection and transmission coefficients obtained in the papers [9,12].

The thermal wave amplitude of the sample surface can be determined using thermal wave interference approach [13]. Using this approach for the surface temperature of the sample and notations of this report we can write

$$\hat{T}_1(k_x,k_y,0,\omega) = \frac{\alpha \hat{I}_p \hat{T}_{1g}}{2q_1 K_1 (1-\hat{R}_{1g}\hat{R}_{12}e^{-2q_1 d})} \int_0^d dz \left[e^{-q_1 z} + \hat{R}_{12} e^{-q_1(2d-z)} \right], \tag{15}$$

where $\hat{T}_{1g} = \frac{2}{1+\xi_{1g}}$ is the transmission coefficient for a thermal wave from the sample region incident on the sample - gas boundary, $\xi_{1g} = \frac{q_g K_g}{q_1 K_1}$, $\hat{R}_{1g} = \frac{1-\xi_{1g}}{1+\xi_{1g}}$ is the reflection coefficient for a thermal wave on the sample - gas boundary. Substituting the values for transmission and reflection coefficients in eq.(15) one obtains

$$\hat{T}_1(k_x,k_y,0,\omega) = \frac{\alpha \hat{I}_p}{(\alpha^2 - q_1^2)K_1} \times$$
$$\times \frac{(r-1)[1+\xi_{12}(1+R_t)][1-e^{-(\alpha+q_1)d}] + (r+1)[1+\xi_{12}(R_t-1)][1-e^{-(\alpha-q_1)d}]e^{-2q_1 d}}{(1+\xi_{1g})[1+\xi_{12}(1+R_t)] + (1-\xi_{1g})[1+\xi_{12}(R_t-1)]e^{-2q_1 d}}, \tag{16}$$

where $r = \frac{\alpha}{q_1}$.

This expression for the surface temperature of the sample coincides with the ones given by eq.(10.2). For the case of $R_t = 0$ eq.(16) coincides also with the result obtained in the papers [12,14].

The photoacoustic gas microphone and photodeflection signals can be determined on the base of eqs.(8),(9) and (10),(16). Silicon nitride ceramics is slightly anisotropic material. Thermal conductivity of the hot pressed silicon nitride ceramics is 0.344 W/cm°C parallel to the hot pressing direction and 0.252 W/cm°C perpendicular to the hot pressing direction at 24°C. Therefore, for preliminary computer simulations an isotropic model was used. This limitation is not principal and anisotropy of material can be taken into account in more detailed calculations.

Some results of calculation of the photoacoustic and photodeflection signals dependence on thermal resistance are shown in Fig.2. The results demonstrate that for $R_t \leq 1$ these methods have approximately linear dependence on R_t. In accordance with these calculations the amplitude of the normal deflection and phase of the photoacoustic signal are the most sensitive to the thermal resistance. Both amplitude and phase of the transverse photodeflection signal have the lowest sensitivity to the thermal resistance between layers.

The influence of the absorption coefficient of the pump beam light on the photoacoustic and photodeflection signals for two modulation frequencies is shown in Fig.3. It is seen that absorption of the pump light does not influence essentially on the sensitivity of these methods at $\alpha \geq 10^3 cm^{-1}$.

The obtained theoretical results can be used also for the estimation of the optimal lateral offset between laser beams for detection of the photodeflection signal. In our case the probe beam radius was 42 μm, pump beam radius 2 μm, height of the probe laser beam was about 160 μm. Under these conditions for frequency range 1 - 3 kHz this optimal lateral offset for transverse component of the photodeflection signal lies in the range 20 - 100 μm.

Experimental Set - up and Results

In this work a self - constructed set - up for photothermal microscopy of solids has been used. Argon - ion laser LGN - 503 of 1 W cw power was used as a heating beam source. Heating beam was modulated by an acoustic - optical modulator ML - 201. In all experiments with imaging the pump beam diameter on the sample surface did not exceed 5 μm. He - Ne laser Meles Griot 05 - LHP - 151 was used as a probe beam source. The probe beam deflection is measured with a silicon position sensitive detector FD - 19 and a selective voltmeter V6 - 9. In piezoelectric experiments a PZT ceramic transducer was used for acoustic signal detection. The phase of the signal was measured by a phasemeter F2 - 16. The sample was mounted on an X - Y translation stage with a minimum step of 5μm. All of these devices except of He - Ne Meles Griot laser were manufactured in the Former Soviet Union. To control the X - Y translation and data processing a computer IBM PC 486 was used.

For estimation of the pump beam light penetration depth in silicon nitride ceramics dependencies on modulation frequency of normal and transverse components of the photodeflection signal and lateral offset have been investigated. These measurements have been performed by using homogeneous region of the sample. The experimental dependence of the normal photodeflection signal on modulation frequency in the range 1 - 20 kHz has been measured. For fitting experimental and theoretical results the computer program was used. This program has been successfully used for determination of thermal parameters of solids [16]. For the case of silicon nitride ceramics the value of the absorption coefficient of the pump laser light was varied. In accordance with this procedure the minimal mean squared error between experimental and theoretical results was obtained at $\alpha > 3 \cdot 10^3$ cm^{-1}. Therefore, for the pump Argon - ion laser with λ = 0,512 μm the depth of the pump beam light penetration in silicon nitride ceramics did not exceed 4 μm.

For an estimation of lateral crack parameters the dependence of the normal photodeflection signal on modulation frequency has been measured. This measurement has been performed for one position of the pump laser beam near indentation 1. The investigated point was situated approximately on the median between radial cracks situated on the right side from indentation. The distance between this point and the center of indentation was about 60 μm. In this procedure the thermal resistance and depth of the crack were fitted. The minimal mean squared error was obtained at R_t = 0.27cm^2·°C/W and d=22μm. Experimental data and theoretical results of fitting for the phase of the normal photodeflection signal are shown in Fig.4. If we use for the relation $R_t \approx d/K_g$, where K_g is the thermal conductivity of the air under normal conditions, then for the crack opening we obtain the value 0,6 μm.

Photodeflection imaging of indents has been performed both by using normal and transverse components of the photodeflection signal. Images 64 x 64 of indents 1 and 2 of row 3 with 20 Kg load obtained by using photodeflection method are presented in Figs.5 - 10 . For the indent 1

normal and transverse deflection images have been obtained at frequency 1 kHz. For the indent 2 these images have been obtained at frequencies 1 and 3.5 kHz. For all images the step of X - Y scan was 5 μm and the offset between laser beams was 22 μm. It is seen that normal photodeflection signal is more sensitive to the lateral crack system while it has some sensitivity to the vertical cracks. Therefore, these images to some extent are similar to the photoacoustic gas microphone images.

In contrast transverse deflection images of indents in silicon nitride ceramics are very sensitive to the vertical cracks. At the same time this component is still sensitive to the lateral crack because of for chosen frequencies the length of thermal waves was comparable with the depth of the lateral crack. However this sensitivity of transverse deflection images to the lateral crack is lower than that of normal deflection images. This result corresponds to the theoretical predictions.

Piezoelectric image 64x64 of indentation 1 of row 3 has been obtained at frequency 57.3 kHz. This image is shown in Fig.11. It is apparent that photoacoustic piezoelectric images highlight different features of the indents. This image reveal the radial and lateral crack system near indentation. Additionally it is clearly seen a structure with fourfold symmetry. This structure is absent on photodeflection images and similar to images of SiC whisker - reinforced alumine ceramics obtained by scanning electron acoustic microscopy [15]. In that paper it was shown that this structure is due to residual stress fields near indentation. Therefore, it is reasonable to consider that we have detected at frequency 57.3 kHz residual stress field in silicon nitride ceramics by the photoacoustic piezoelectric method.

Conclusions and Recommendations

The obtained theoretical and experimental results demonstrate that photoacoustic gas microphone, photodeflection and piezoelectric methods could be a base for a complex approach to the problem of indentation crack imaging in silicon nitride ceramics. In this case gas microphone and normal deflection could be used for detailed investigation of lateral cracks. Transverse component of the deflection signal in this approach could be used for imaging of vertical cracks (radial, median, half - penny). However, for quantitative photothermal imaging of vertical cracks in silicon nitride a detailed theoretical model should be developed.

The obtained photoacoustic piezoelectric image clearly demonstrated residual stress fields in silicon nitride ceramics near indentation. Therefore, it is reasonable to use this method for residual stress fields imaging in ceramics than more complicated scanning electron acoustic microscopy. It seems also reasonable to perform photoacoustic piezoelectric investigation of residual stress fields in silicon nitride in combination with the heat treatment of the sample.

In conclusion, we have demonstrated that photoacoustic gas microphone, photodeflection and piezoelectric methods could be a base for lateral, vertical cracks and residual stress field imaging in silicon nitride ceramics.

Literature Cited

1. A.G.Evans, E.A.Charles, "Fracture Toughness Determination by Indentation", J. Am.Ceram. Soc., **59**, 371 - 372 (1976)
2. R.F.Cook, G.M.Pharr, "Direct Observation and Analysis of Indentation Cracking in Glasses and Ceramics", J. Am. Ceram. Soc., **73**, 787 - 817 (1990)
3. P.K.Kuo, L.J. Inglehart, L.D.Favro, R.L.Thomas, 1981 Ultrasonics Symposium, IEEE, 837 - 839 (1981)

4. P.K.Kuo, L.J.Inglehart, L.D.Favro, R.L.Thomas, "Photoacoustic Phase Signatures of Closed Cracks", J. Appl. Phys., **53**, 1258 - 1260 (1982)
5. D.N.Rose, D.C.Bryk, G.Arutunian, J.E.Dumar, M.J.Slavin, "Photoacoustic Microscopy of Indentation Lateral Cracks", J. de Physique IV, Colloque C7, Suppl. an de Phys.III, **4**, 599 - 602 (1994)
6. J.Rantala, J.Hartikainen, J..Jaarinen, "Photothermal Determination of Vertical Crack Lengths in Silicon Nitride", Appl. Phys. A, **50**, 465 - 471 (1990)
7. R.M.Burbelo, A.L.Gulyaev, L.I.Robur, M.K.Zhabitenko, B.A.Atamanenko, Ya. A.Kryl, "Photoacoustic Visualization of Residual Stress in Ceramic Material", J. de Physique IV, Colloque C7, Suppl. au J. de Phys. III, **4**, 311 - 314 (1994)
8. D.O.Ajai, K.C.Ludema, Wear, **124**, 237 - 357 (1988)
9. F.Lepoutre, D.Fournier, A.C.Boccara, "Influence of 3-D Effects on the Contrast in Photothermal Imaging", in "Nondestructive Characterization of Materials II", Ed. by J. F. Bussiere et al., Plenum Press, New York, N.Y., 771 - 775 (1987)
10. A.L.Glazov, K.L.Muratikov, "Photodeflection Signal Formation in Thermal Wave Spectroscopy and Microscopy of Solids within the Framework of Wave Optics. "Mirage" Effect Geometry", Opt. Comm., **84**, 283 - 289 (1991)
11. A.Glazov, K.Muratikov, "Simulations of Photodeflection Measurements of Thermal Diffusivity of Solids: Wave Optics Approach", J. Appl. Phys., **76**, 3279 - 3284 (1994)
12. D.N.Rose, G.H.Quay, W.Jackson, and S.L.Anderson, "An Introduction to One Dimensional Single Layer Thermal Wave/Photoacoustic Theory", TARDEC University Press, Warren, Michigan (1994)
13. C.A.Bennet, R.R.Patty, "Thermal Wave Interferometry: A Potential Application of the Photoacoustic Effect", Appl. Opt., **21**, 49 - 54 (1982)
14. A.Rosencwaig, "Photoacoustics and Photoacoustic Spectroscopy", Wiley and Sons, New York, N.Y. (1980)
15. J.H.Cantrell, M.Qian, M.V.Ravichandran, K.M.Knowles, "Scanning Electron Acoustic Microscopy of Indentation - Induced Cracks and Residual Stresses in Ceramics". Appl. Phys. Lett., **57**, 1870 - 1872 (1990)
16. K.L.Muratikov, A.L.Glazov, "Measurement of Thermophysical Parameters of Bulk Materials by a Photodeflection Method", Tech. Phys. Lett., **21**, 876 - 878 (1995)

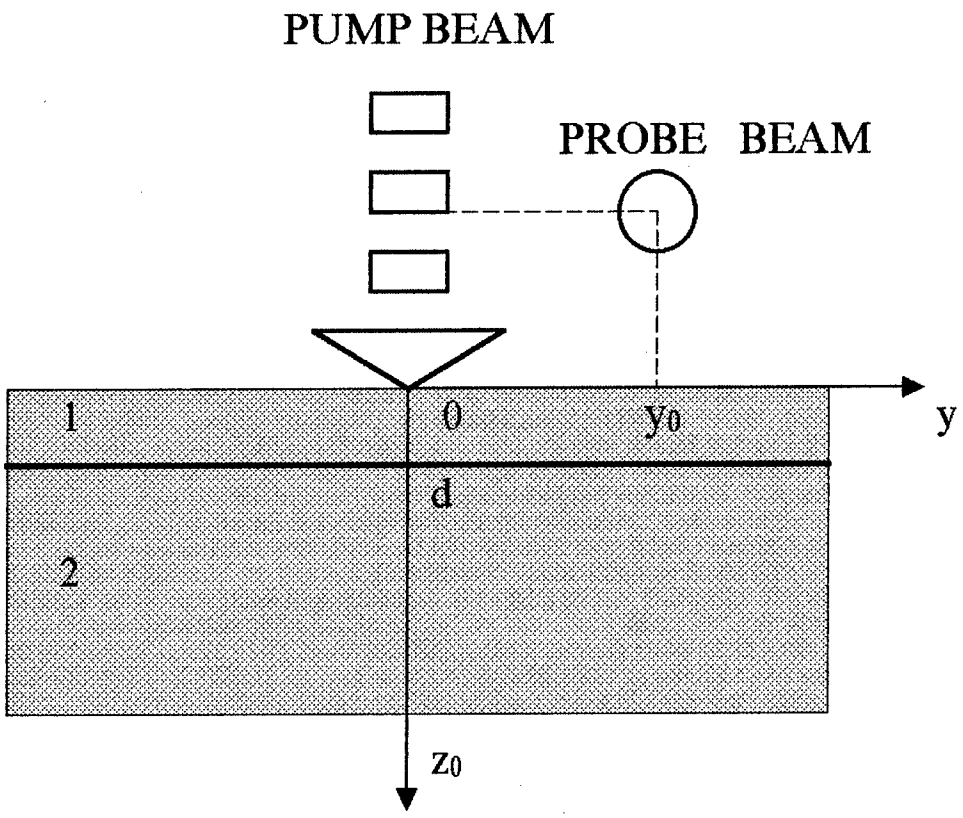

Figure 1. The scheme of the photodeflection experiment.

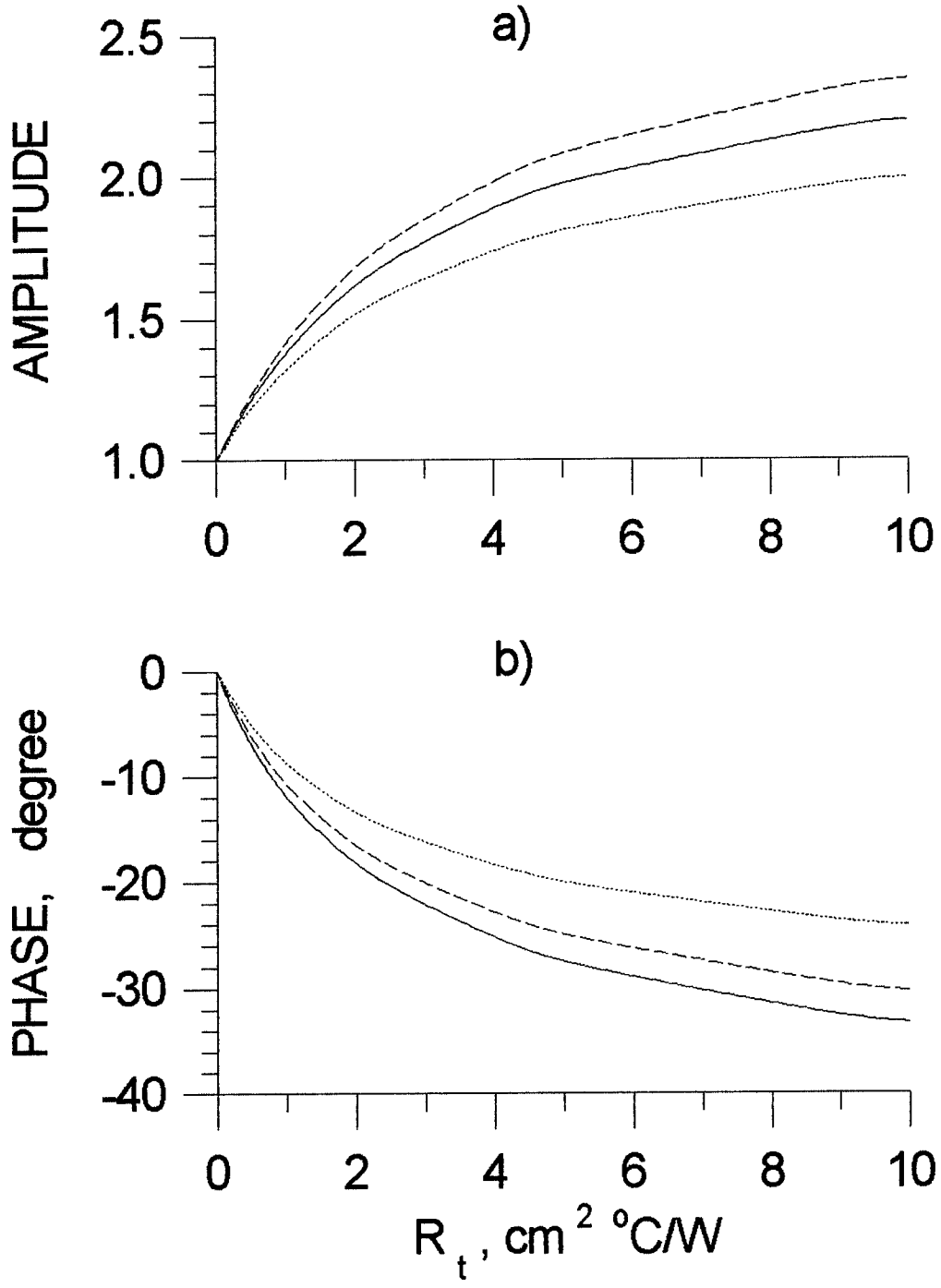

Figure 2. The dependence of photothermal signals on the thermal resistance. a) is the amplitude component devided on the amplitude of signal at $R_t = 0$, b) is the phase component minus that at $R_t = 0$. Solid curve corresponds to the photoacoustic signal, dash curve corresponds to the normal component of the photodeflection signal, dotted curve corresponds to the transverse component of the photodeflection signal. The signals were calculated at the probe beam radius of 42 μm, the pump beam radius of 2 μm, the vertical offset of the probe beam of 156 μm and the lateral offset of the probe beam of 100 μm.

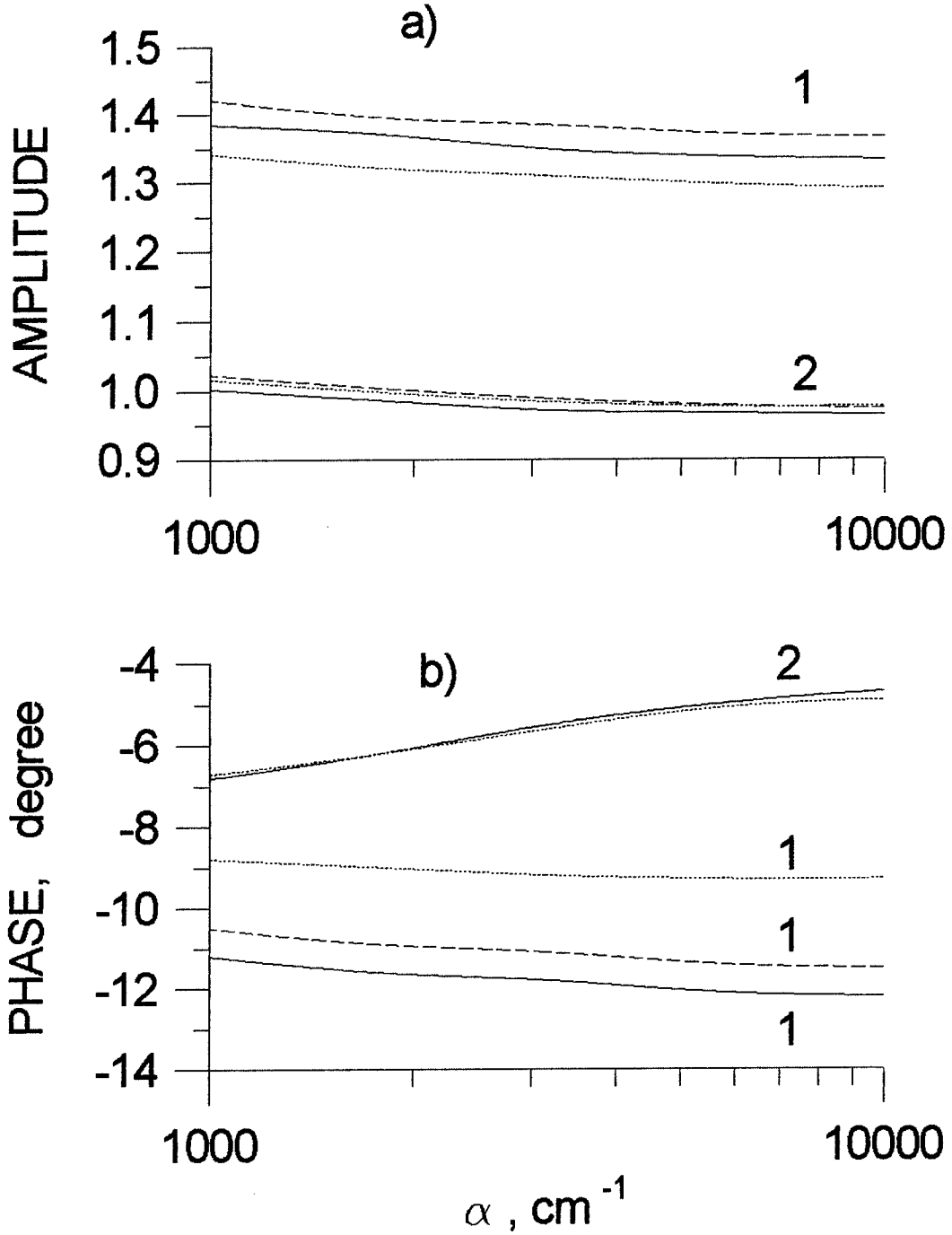

Figure 3. The dependence of photothermal signals on bulk absorbtion of the pump beam. a) is the amplitude component devided on the amplitude of signal at $R_t = 0$, b) is the phase component minus that at $R_t = 0$. Solid curve corresponds to the photoacoustic signal, dash curve corresponds to the normal component of the photodeflection signal, dotted curve corresponds to the transverse component of the photodeflection signal. Numbers 1 and 2 correspond to modulation frequencies 1 and 10 kHz. The signals were calculated at the probe beam radius of 42 μm, the pump beam radius of 2 μm, the vertical offset of the probe beam of 156 μm and the lateral offset of the probe beam of 100 μm.

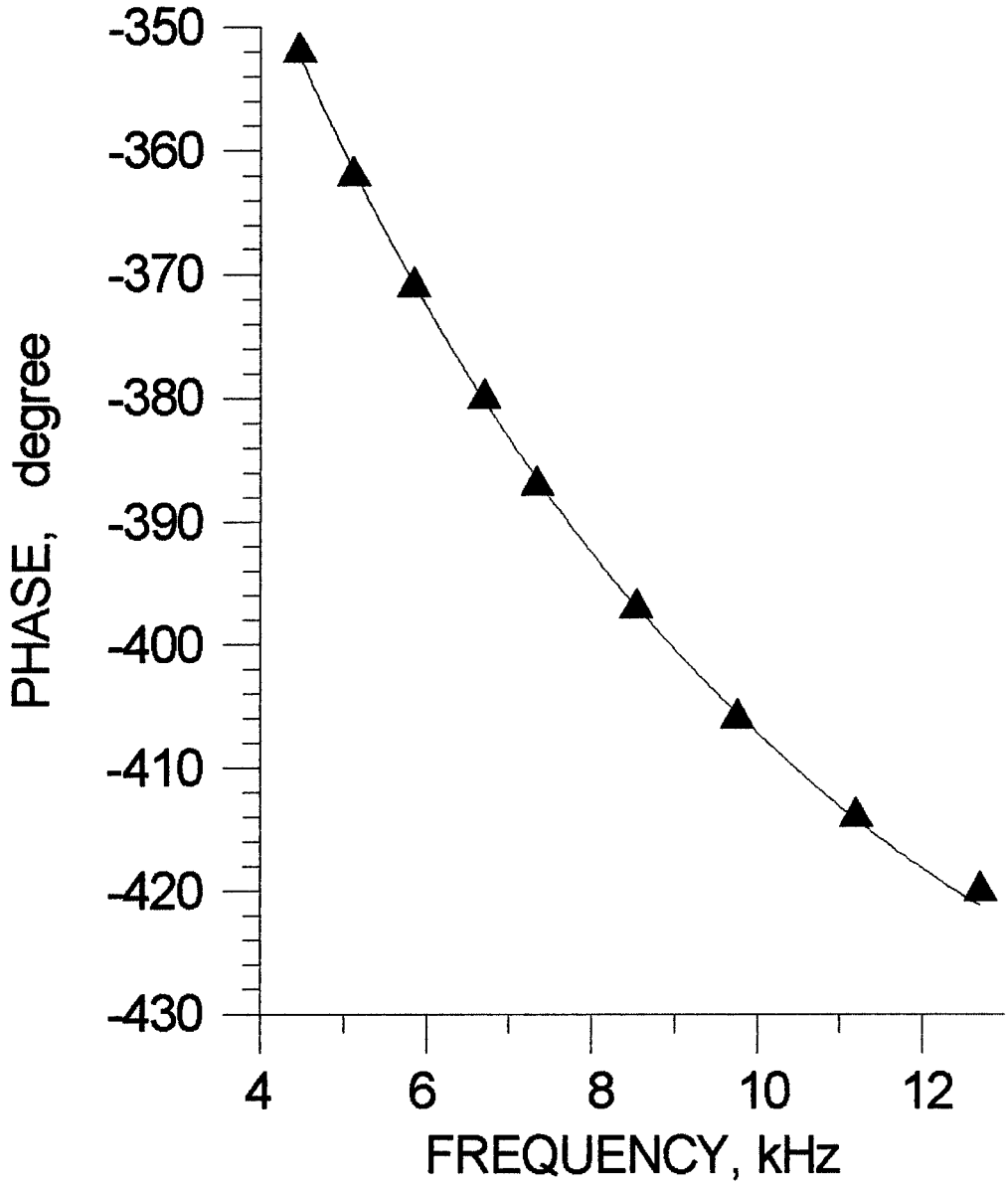

Figure 4. The result of fitting the crack depth and thermal resistance for the phase of the normal photodeflection signal. ▲ - experimental points, ——— - theoretical result. Experimental parameters are the probe beam radius is 42 μm, the pump beam radius is 2 μm, the vertical offset of the probe beam is 156 μm, the lateral offset of the probe beam is 15 μm.

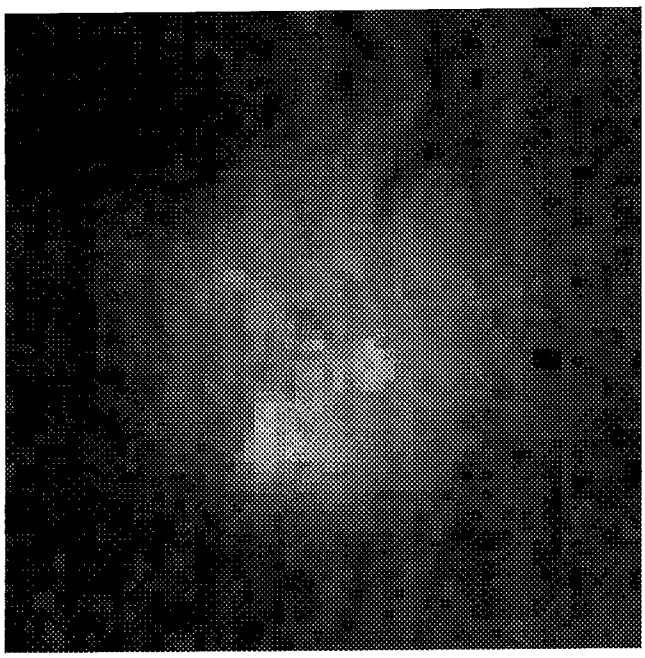

a

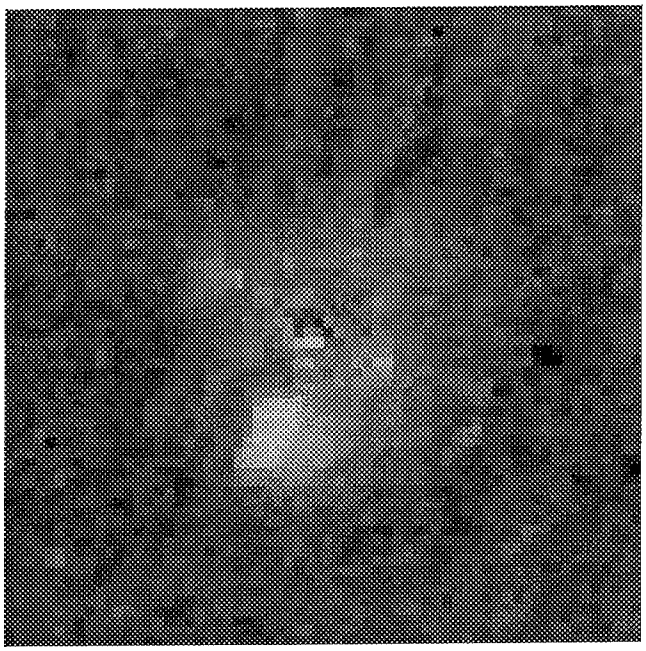

b

Figure 5. The photodeflection image of indentation 1 of row 3. The normal component of the signal (a - is the amplitude, b - is the phase). The modulation frequency is 1 kHz, the lateral offset is 22 μm.

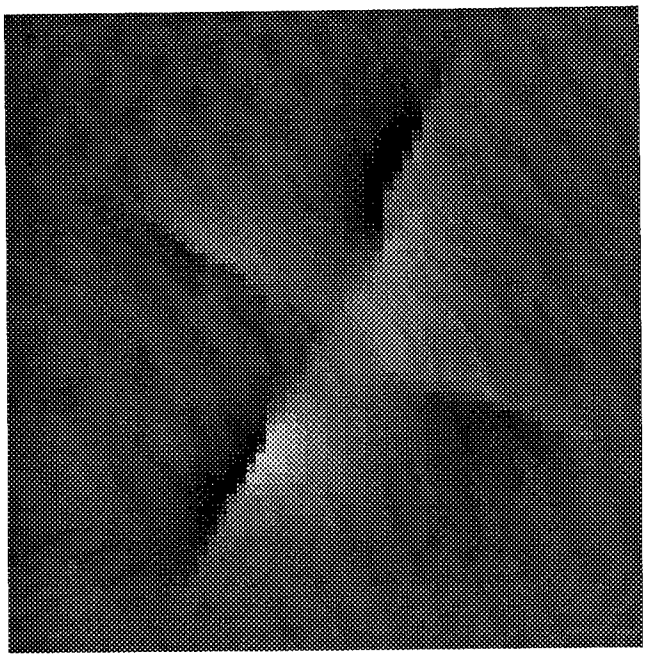

a

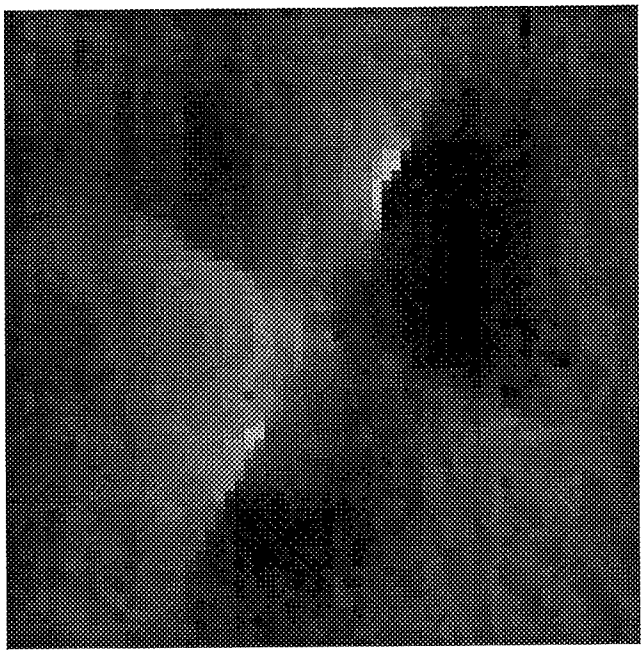

b

Figure 6. The photodeflection image of indentation 1 of row 3. The transverse component of the signal (a - is the amplitude, b - is the phase). The modulation frequency is 1 kHz, the lateral offset is 22 μm.

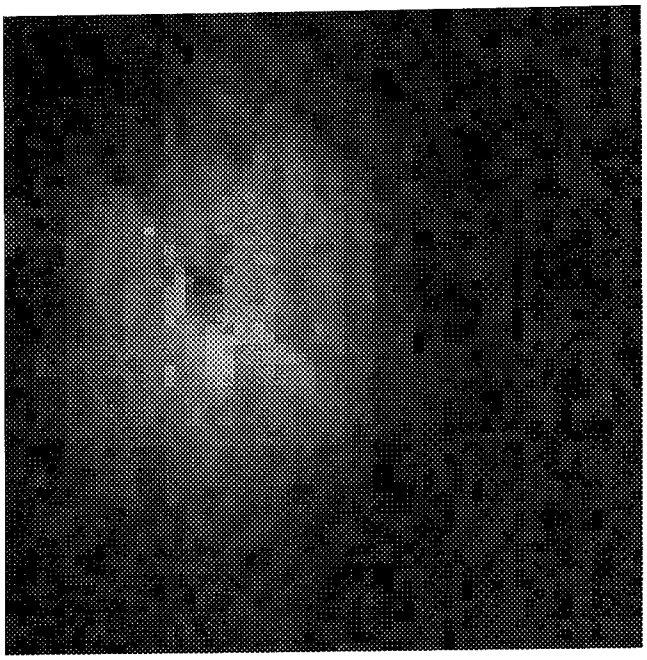

a

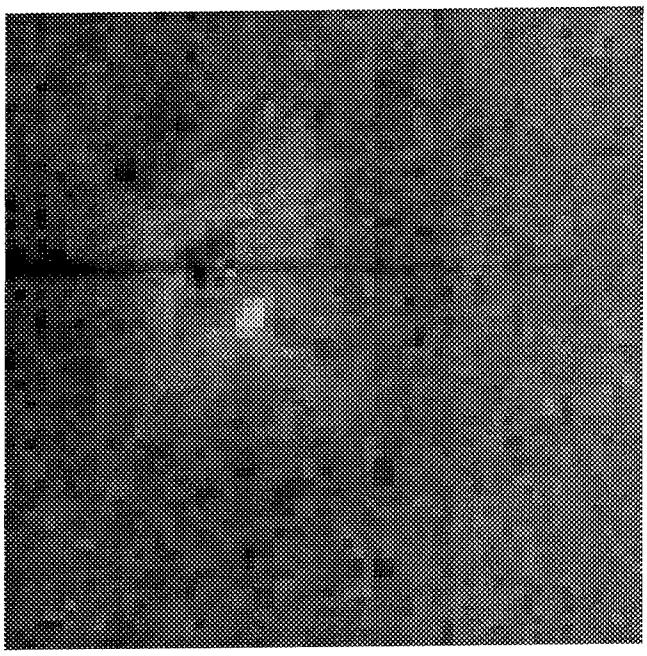

b

Figure 7. The photodeflection image of indentation 2 of row 3. The normal component of the signal (a - is the amplitude, b - is the phase). The modulation frequency is 1 kHz, the lateral offset is 22 μm.

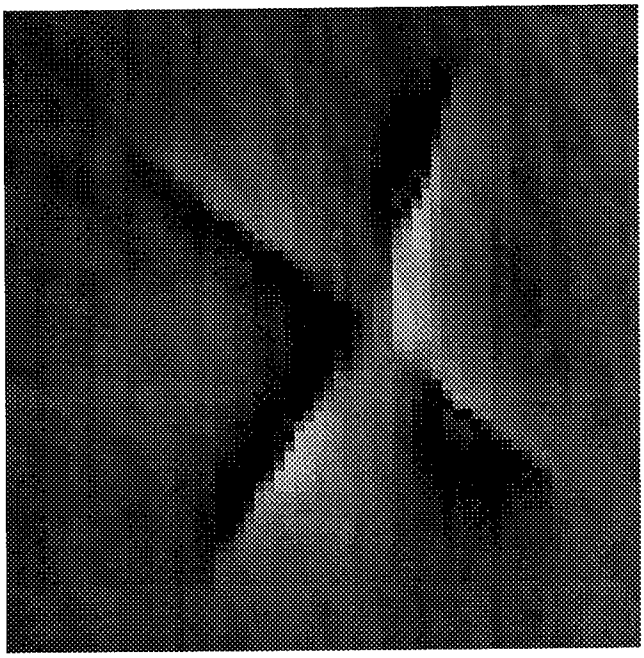

a

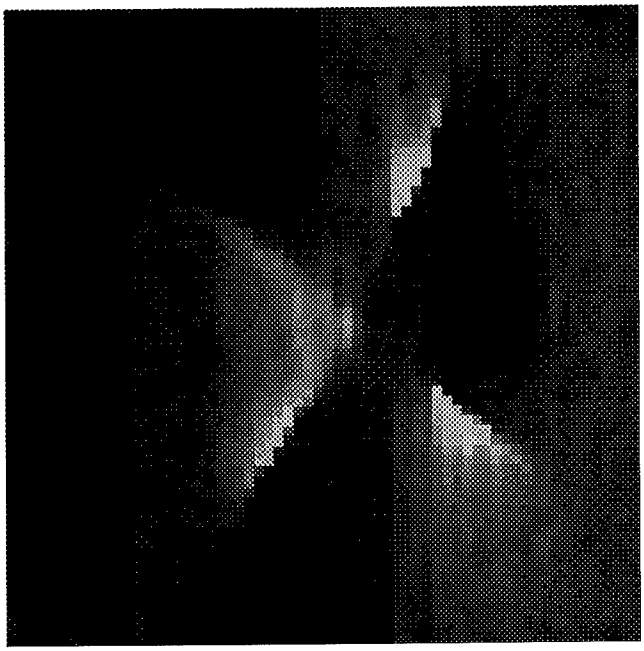

b

Figure 8. The photodeflection image of indentation 2 of row 3. The transverse component of the signal (a - is the amplitude, b - is the phase). The modulation frequency is 1 kHz, the lateral offset is 22 μm.

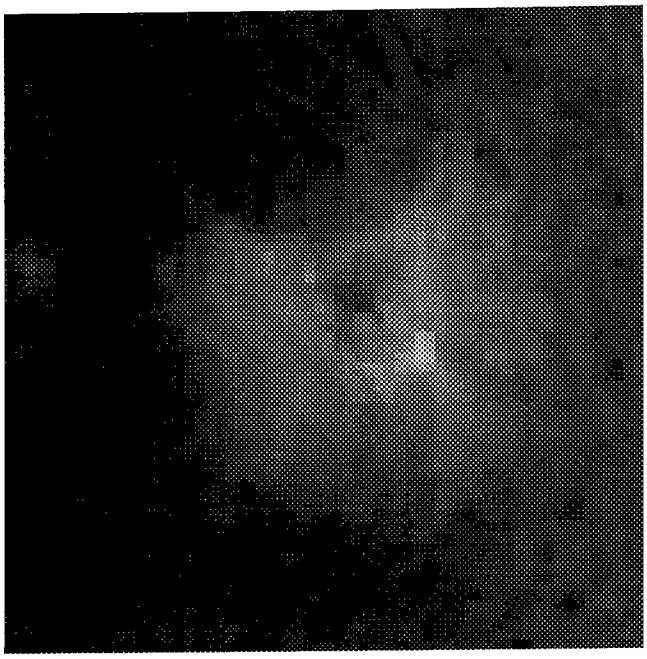

a

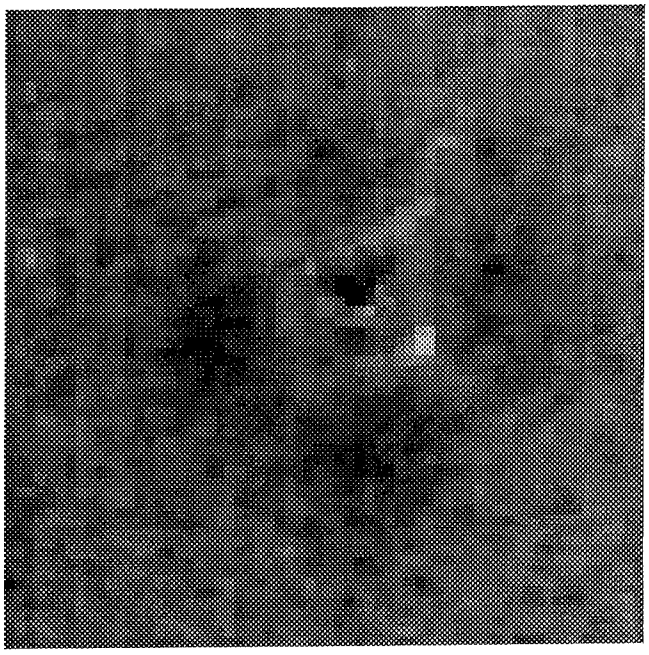

b

Figure 9. The photodeflection image of indentation 2 of row 3. The normal component of the signal (a - is the amplitude, b - is the phase). The modulation frequency is 3.5 kHz, the lateral offset is 22 μm

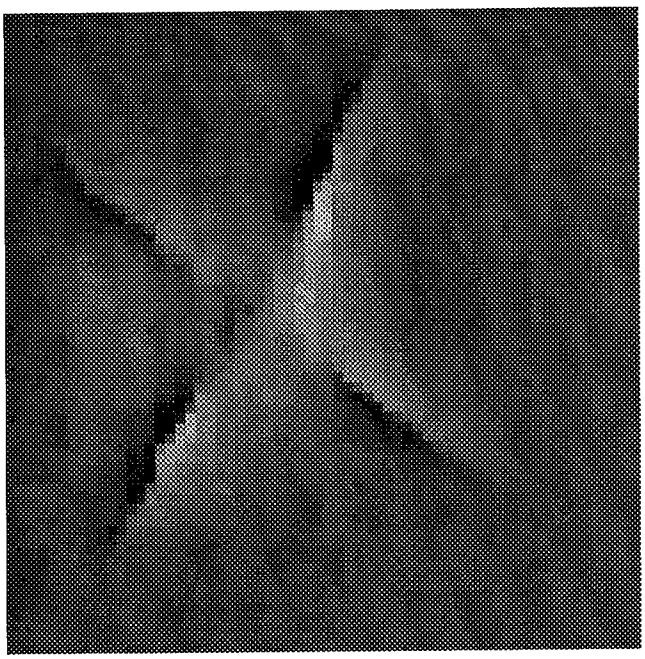

a

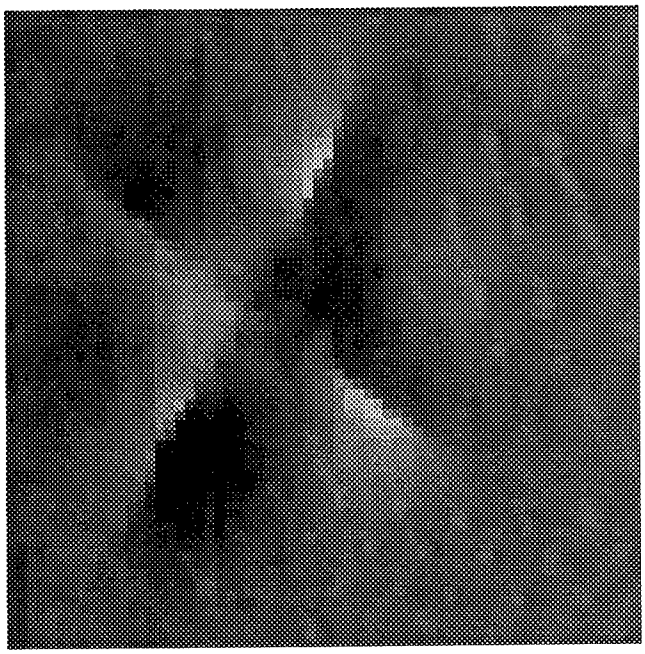

b

Figure 10. The photodeflection image of indentation 2 of row 3. The transverse component of the signal (a - is the amplitude, b - is the phase). The modulation frequency is 3.5 kHz, the lateral offset is 22 μm.

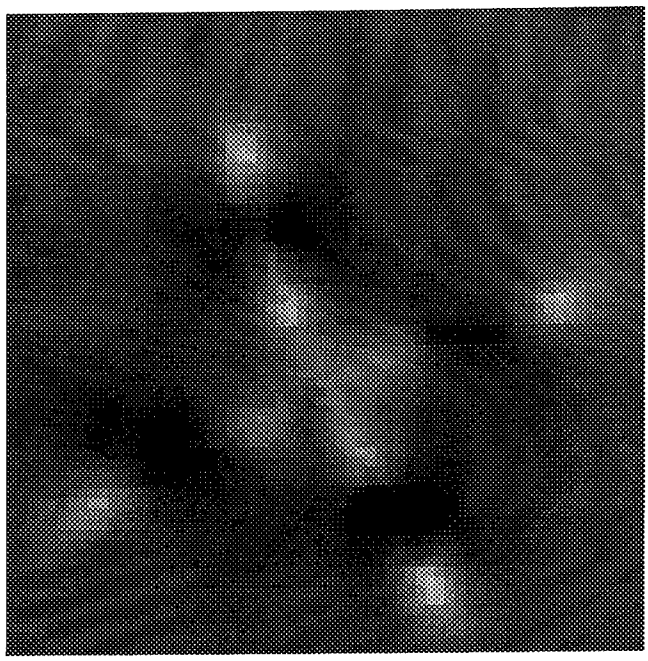

a

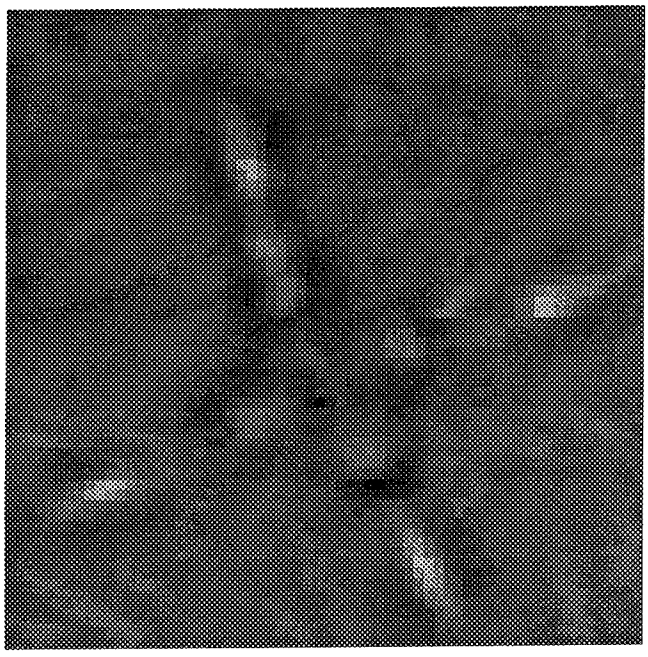

b

Figure 11. The piezoelectric image of indentation 1 of row 3 (a - is the amplitude, b - is the phase). The modulation frequency is 57.3 kHz.